CRLH ZOR theory, design and microwave applications

MOHAMED M. MANSOUR[*], MOSTAFA A. ELMALA, ABDEL-AZIZ T. SHALABY[a], EL-SAYED M. EL-RABAIE[a]
Electronics Research Institute, Dokki, Giza, Egypt
[a]Department of Electronics and Communication Engineering, Faculty of Electronic Engineering, Menouf-32952, Egypt

In this article, a survey about ZOR is illustrated and its characteristics are investigated in a detailed manner. The fabrication process has been presented to focus on the practical limitations of metamaterials. An application based on ZOR like a notch filter is presented. The notch filter is used in UWB applications. Later, a tunable mechanism based on the nonlinear dielectric of ferroelectric has been proposed. The model is only simulated and tested with published measured data. All different configurations were designed with both HFSS and CST, what resolve the electromagnetic fields in all the structure that is going to be analyzed.

1. Introduction

The idea of left-handed materials and negative refraction first arose during the 1960s when a Russian physicist Victor Veselago considered optical properties of a hypothetical material. It is well known that, in general, any material's response to applied electromagnetic radiation can be characterized by two electromagnetic parameters, magnetic permeability and electric permittivity. Typically, these quantities are positive. In a paper published in 1968, Veselago considered a material whose permeability and permittivity become simultaneously negative, and termed it as left-handed material, because the electric and magnetic fields form a left-handed set of vectors with the wave vector [1]. When ε and μ are both negative, there are dramatically new properties.

In 2001, Smith and his team in San Diego demonstrated the first artificially fabricated metamaterial [2] that has peculiar property of left-handed materials: it bends electromagnetic waves in the opposite direction to normal materials. These properties have enabled the development of new concepts and devices and possible utilization in many novel applications [3-7]. Zeroth-order resonator (ZOR) is one of the novel applications of LHMs. Such LHM based resonators can have arbitrary designed resonant frequencies that are independent on their physical lengths. Hence they can be very compact, especially at lower frequencies. Examples of such resonators have been reported in [8-9], where gap coupled LH TL ZORs formed by cascading LH unit cell TLs in microstrip and CPW configurations were presented.

In this paper, we focus on the miniaturization of ZOR size to an order comparable less than the design found in Ref. [8]. The typical design of ZOR depends on a series capacitor either an MIM or IDC and a parallel inductor like a stub-shorted inductor. Our design has been fabricated using the MIM and the stub components to constitute the left-handed TL resonator. For UWB notch filter, we present an essential design for rejecting the narrowband signal which conveys the band 3.4 to 3.6 GHz range. At the end, a tunable a CRLH metamaterial ZOR is explained using the properties of ferroelctric materials.

The paper is organized as follow, Sec II provides the ZOR design principle and architecture, Sec III pointed out the proposed application of ZOR in UWB, Sec IV shows the effect of inserting a thin film ferroelectric material in the ZOR response and Sec V concludes the paper with a brief summary of the work done.

2. ZOR design principle

A. Operating principle of a CRLH ZOR

In conventional RH TL resonators, the propagation constant is always positive, and hence a conventional RH TL resonator can only resonate at infinite positive order modes. A novel LH TL resonator has been introduced as an application of the LH TL theory. The principle of its operation is based on cascading a LH TL section and a RH one [10]. The total phase shift of the TL can be expressed as the sum of LH and RH phase shifts, i.e.

$$\beta l = \beta_l d_l + \beta_r d_r \qquad (1)$$

Where β_l and β_r are the propagation constants of LH and RH sections, respectively, whereas d_l and d_r represent the lengths of these sections, respectively, while l is the total length of the combined line.

A LH resonator can have either positive, negative, or zero phase shifts according to the combination of its left/right handed TL sections. LH ZOR is a unique TL

resonator that could not exist in nature. Its resonant condition is based on achieving zero propagation constant due to the phase compensation of the LH and RH TL sections [6].

The resonant frequency of the LH ZOR depends on the length ratio of the LH and RH TL sections and it is independent on the total physical length of the resonator, meaning that the resonant frequency can be determined by both the LH and RH loading elements. Since the LH TL itself has unavoidable RH effects due to its parasitic series inductance and shunt capacitance [6], the RH loading elements can be realized by carefully utilizing the RH parasitic effects of the LH TL. A ZOR has zero electric length (hence infinite guided wavelength) at a certain finite microwave frequency with very small size.

B. CRLH ZOR structure

The cell of ZOR is constituted with a series MIM capacitor which represent C_L and a shunt stub inductor which represent L_L and both generate the LH section of CRLH, a series transmission line will constitute the RH section of CRLH. Fig. 1 shows the unit cell of this resonator (which is the implemented prototype layout).

The structure mimics the conventional CRLH unit cell, where is provided by the MIM capacitor with area ($w_m * l_l$), $L_R / 2$ is provided by the narrow trace of width w_t and length l_t with the width discontinuities, L_L is provided by the via-grounded stub inductor of length l_s and width w_s, and C_R is provided by the trace-to-ground voltage gradient.

The ZOR architecture is shown in Fig. 1, and consists of two-layer substrate with $\varepsilon_{r1} = 2.2$, $\varepsilon_{r2} = 2.94$ and height $h_1 = 0.8mm$, $h_2 = 0.1mm$ at central frequency of 2.2 GHz.
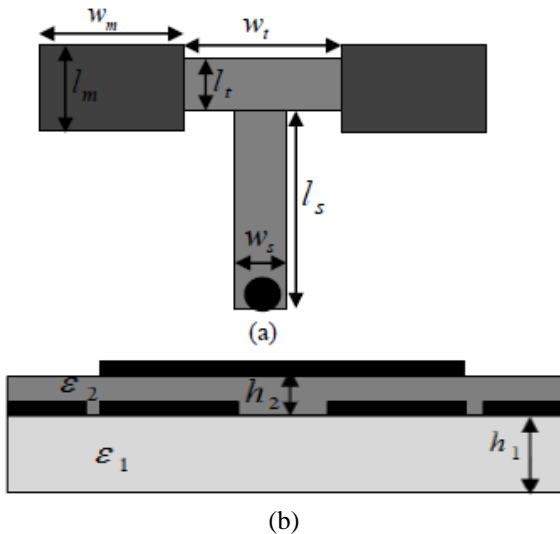

(a)

(b)

Fig. 1. Unit cell of a CRLH LH (a) Upper view
(b) Cross-sectional view.

The equivalent circuit topology is shown in Fig. 2. The parameters values are selected to obtain the optimum matching condition at the input and output port.
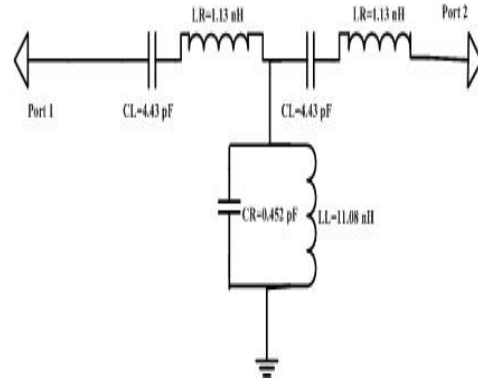

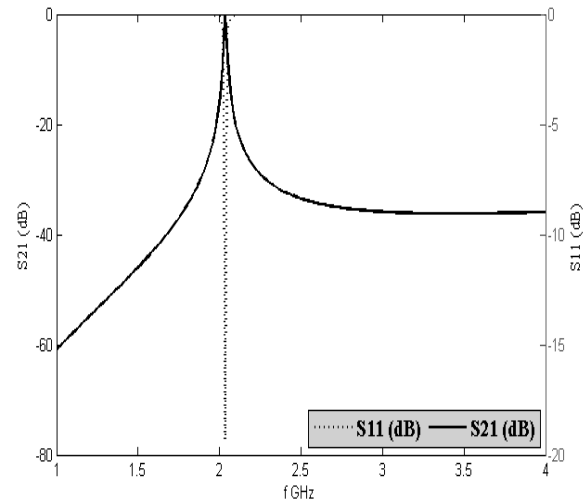*Fig. 2. Lumped Equivalent Circuit of unit cell ZOR shown in Fig. 1.*

Fig. 3. Agilent ADS circuit simulation.

As we see from the output of circuit simulation, the selected structure parameters are closely matched with our calculations for designing the ZOR CRLH structure as shown in Fig. 3.

The full wave analysis and measurement results are given in Fig. 4. As we see, the measured results agree reasonably with those acquired from the circuit analysis and full-wave simulations. The measured insertion loss is larger than simulated due to the inherent losses of various sources as dielectric, conductor and radiated as well as the connector losses. The dip in the S11 response at 2.2 GHz is explained by the unbalance of the CRLH structure induced by imperfections of the fabricated prototype, including mostly inaccuracy in the location, width of the thickness of the via holes and the misalignment of the two layers.
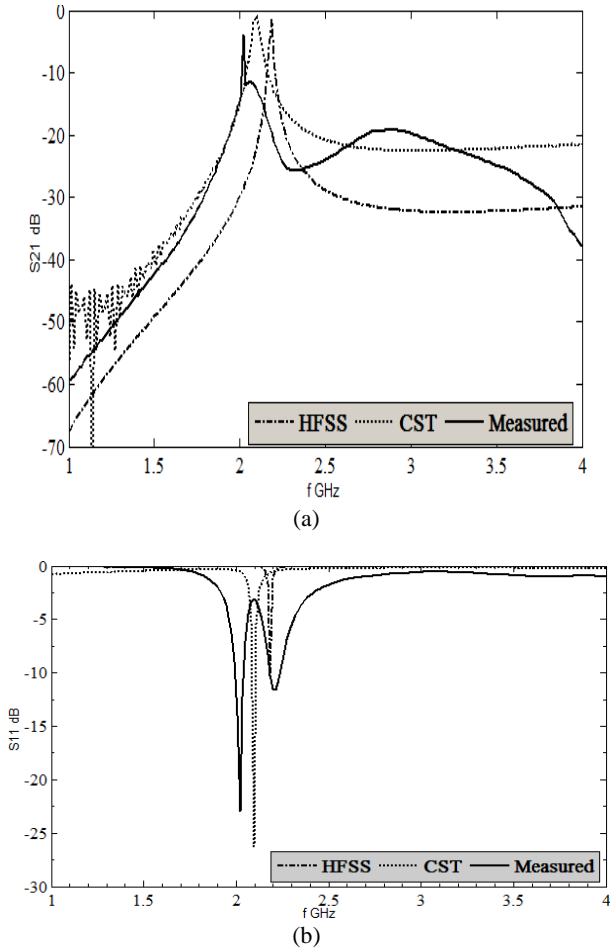
Fig. 4. Simulated and measured results for the CRLH ZOR.
a)   Insertion loss S_{21}.   (b) Return Loss S_{11}.

A Comparison between the proposed structure in this paper and the one in [3] is given in Table 1.

Table 1. Comparison between the design parameters in reference [3] and those in this paper.

Parameter	IDC Simulated [3]	MIM (Simulated)	IDC Measured [3]	MIM (Measured)
Size (mm²)	240	120	240	120
S_{11} (dB)	-14	-26	-6.8	-22
S_{21} (dB)	-2	-0.92	-3	-4
Spurious Resonances	Yes	No	Yes	No
Q	250	250	250	250

As shown from the above comparison, the structure proposed in [3] has a size of (24.6*9.9 mm²) which is larger than the one discussed in this paper by about 47%. Also the one in [3] suffers from; the multiresonance

introduced by the interdigital capacitor and the complexity of its design.

3. ZOR application: notch filter

The notch filter principle theory depends on passing all frequencies except a certain band should be rejected i.e. the circuit must behave at those frequencies (notches) as a short circuit. This can be verified by a conventional transmission line that connects the output port to the input port and a resonant circuit is inserted between the transmission line. This resonant circuit resonates at the frequency of interest and we can control the bandwidth by optimizing the circuit components and the dimensions parameters. The resonant circuit is constituted using a ZOR with the above architecture except the capacitor is replaced with IDC and the resonant frequency is shifted to 3.5 GHz which is the central frequency of Wi-MAX 802.16d (3.4 to 3.6 GHz) standard that resides in the UWB (3.1 to 3.9 GHz).

The design of the proposed notch filter is based on a balanced short-ended CRLH transmission line. As shown in Fig. 5(a), the short-ended CRLH transmission line, with characteristic impedance Z_{in} and the propagation constant β, acts as a shunt branch between the input port and output port. When the propagation constant β vanishes at the frequency f_0, Z_{in} is also vanished and the shunt CRLH stub becomes shorted at f_0. Thus, the transmission from port 1 to port 2 vanishes also, which can behave as a notch filter at f_0. The design of our model has been based on this principle.
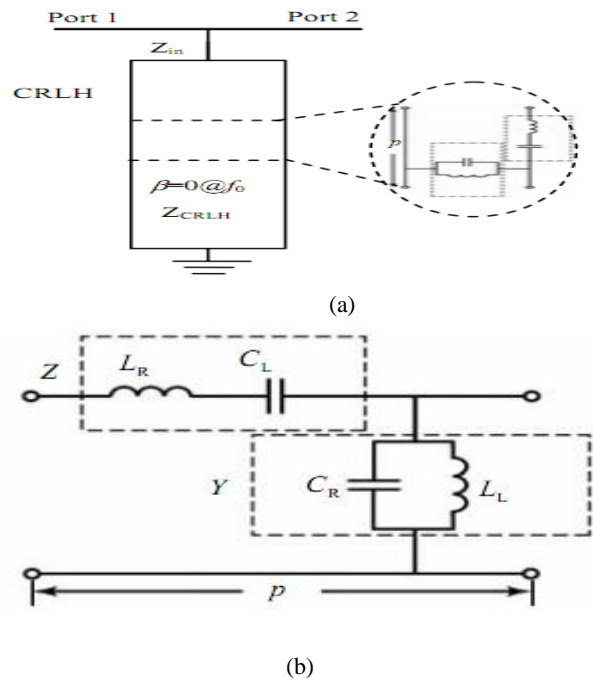

Fig. 5. (a) Structure of the proposed notch filter;
(b) The lumped LC unit cell for the CRLH TL.

Fig. 6 depicts the layout of the UWB notch filter with a wide notch of 200 MHz, which is proposed on the FR4 substrate with permittivity of 4.5 and thickness of 1.5 mm. The microstrip architecture design with interdigital capacitor (IDC) and short-circuited stub on the top side is employed.
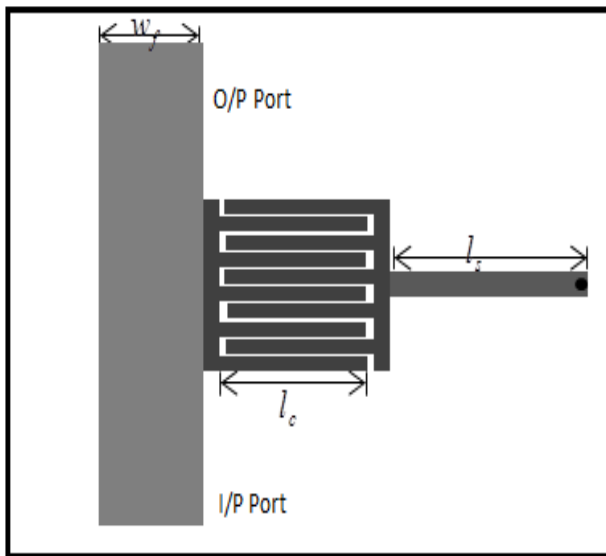

Fig. 6. Layout of the proposed UWB notch filter.

A comparison is made between the simulated results and the measured response is depicted in Fig. 7 a, b. From the comparison of the results, it is clear that:

(1) The measured frequency response almost agrees with the simulated results.

(2) As shown in Fig. 7(a), the insertion loss |S21| has a magnitude of about −30 dB which is verified with the simulated results but the frequency of the notch is slightly shifted towards the high frequency side. This difference between the two notches (the simulated and the measured) is due to the imperfections resulted from the fabrication and SMA connectors.

(3) As shown from Fig. 7(b), the return loss $|S_{11}|$ is 1.0 dB at the frequency 3.5GHz for the simulated response.

(4) The undesired notch appeared at frequency above 4.5 GHz is mainly due to the spurious resonance coming from the inter-coupling between the fingers of IDC.
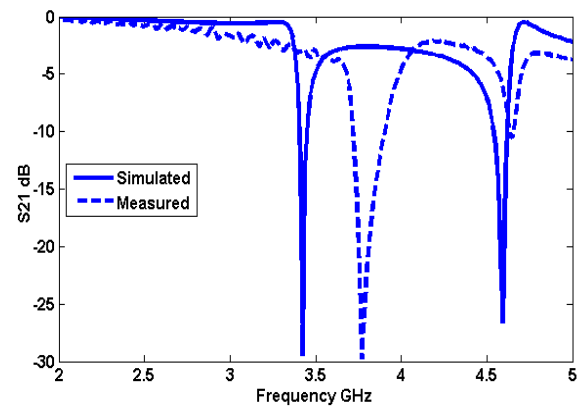
(a)
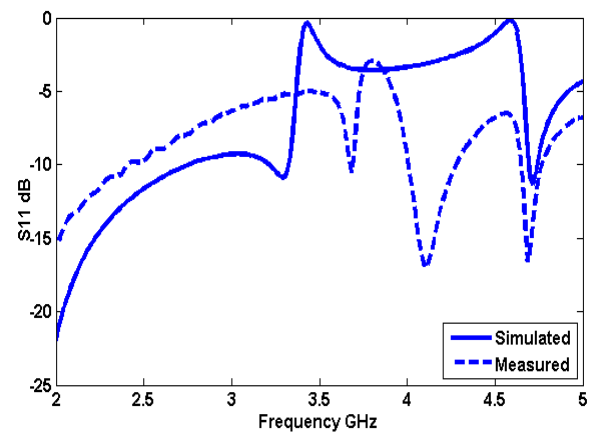
(b)

Fig. 7. Comparison between simulated and measured results: (a) S_{21} response (b) S_{11} response.

The notched band can be controlled by properly selection of the length of the stub, width of the stub, and length of the IDC fingers. A filter with a WLAN notch band is designed, simulated and fabricated. The measured results show close agreement with the simulated results which validates the proposed filter design theory.

4. Tunable ZOR based on ferroelectric materials

A.   Adding HTS

It is known that for most resonant structures, attainment of optimal performance requires some level of additional tuning through either mechanical means or other coupling mechanisms. Therefore, incorporation of electronic   tuning   into HTS   components with- out degradation of performance is very attractive. The result will be low-loss microwave components that could be fine-tuned for optimal performance, with the additional attribute of being tunable over a broadband frequency range. The dielectric properties of the ferroelectric thin

film, and the thickness of the ferroelectric film, play a fundamental role in the frequency or phase tunability and the overall insertion loss of the circuit.

Planar HTS microstrip circuits are attractive for communication applications due to their lower conductor losses com-pared to normal conducting circuits at cryogenic temperatures. Instead of the normal conductor used in Fig. 1, an YBCO thin film [9] is replaced.
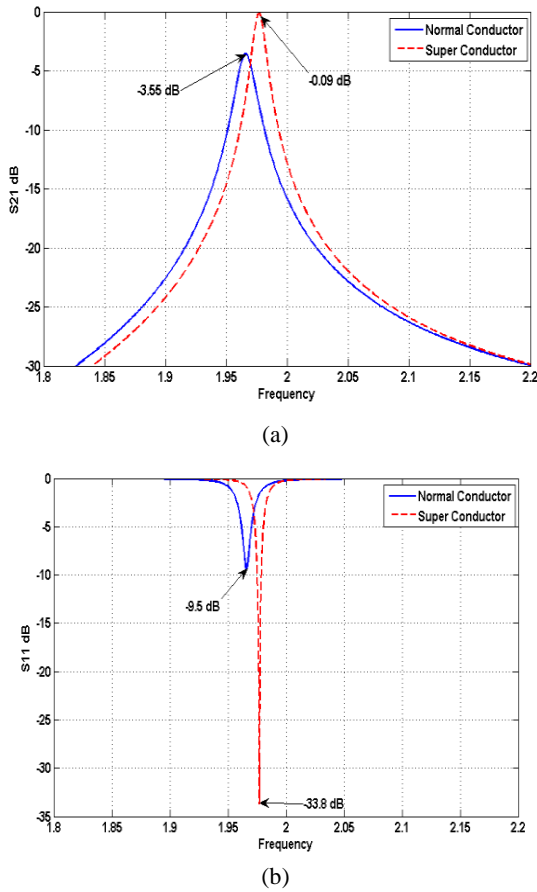

(a)

(b)

Fig. 8. Adding superconductor and comparison with the normal case (a) S_{21}. (b) S_{11}.

As shown in the Fig. 8, with the superconductor insertion, the dissipation in S_{21} is greatly reduced from -3.55 dB to -0.09 dB by a percentage of 97.5 %., and the matching is improved from (-9.5 dB up to -34 dB), and this shares in improving the Q factor to a large extent comparable with the previous case.

B. Adding ferroelectric

Ferroelectric thin films can be easily incorporated into a microstrip structure of CRLH MTM depicted in Fig. 1. Ferroelectric tunable microstrip structures are potentially attractive for frequency-agile microwave communication systems. These tunable components enable a new class of frequency-agile components with large tunabilities and negligible additional losses when combined with

HTS conductor for low-temperature applications. SrTiO3 (STO) thin films with large dielectric tunability and low loss tangents at microwave frequencies have been the most promising ferroelectrics for integration with HTS circuits [12]. The most common ferroelectric tunable structure is based on conductor/ ferroelectric/ dielectric two-layered microstrip.

Ferroelectric/superconductor thin films ($YBa_2Cu_3O_{7-\delta}/Ba_{0.05}Sn_{0.95}TiO_3$) are used to realize an electrically tunable, low-loss composite right/left-handed transmission line. A resistive line is implemented as both DC bias path and RF choke. The whole device maintains an all-planar configuration. The composite right/left-handed transmission lines are well matched showing a wide pass band [13].

The electrical tuning is based on the electric-field dependence of the ferroelectric permittivity. An IDC is used here as the tuning element for its capability, among planar structures, of establishing relatively high electric field between its two electrodes. The ferroelectric thin film is sandwiched between the circuit layer and the substrate. As for biasing, one can either apply through the RF ports using a bias Tee or through an independent bias network with an RF choke. The former approach is advantageous in that it introduces less interference to the main circuit and is often easy to fit into measurement systems. However, due to the high-pass nature of a CRLH-TL, applying DC voltage through the RF ports is not straightforward. Here a resistive line approach is proposed as shown in Fig. 9 for a 3-unit CRLH-TL. The resistive line blocks the RF in the DC path if its resistance is sufficiently high. With such a line of 10 μm wide, the simulated responses for different surface resistances are given in Fig. 10.

The incurred loss is about 0.6 dB for $20\,\Omega$ surface resistances, 0.3dB for $50\,\Omega$, and 0.2dB for $90\,\Omega$, corresponding to a line resistance of over 2, 5, and 9 $K\Omega$ per unit-cell.
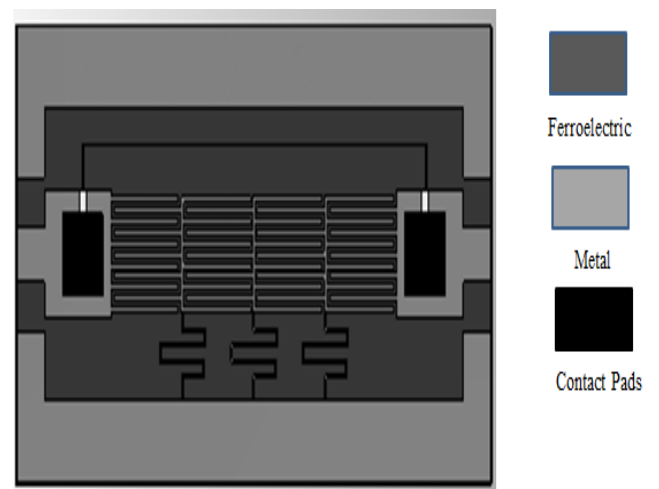

Fig. 9. Layout of a 3-unit CRLH-TL with resistive bias line, IDC and meander line inductor.
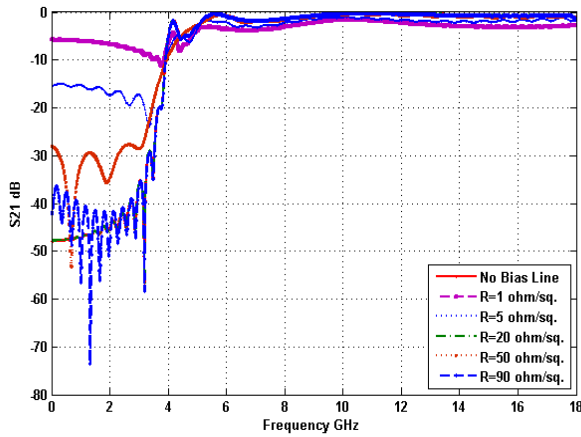
*Fig. 10. Simulated responses of a 3-unit CRLH-TL
with different surface resistances of the bias line.*

The modified microstrip structure of Fig. 2 is depicted in Fig. 11, consists of a dielectric substrate (e.g., LAO or MgO, typically 254 μm to 500 μm thick, we will use LAO with permittivity 23.6, a ferroelectric thin-film layer (thickness varying between 300-2000 nm for various applications), a gold or YBCO thin film (2 μm thick or 300-600 nm thick, respectively) for the top conductor, and a 2 μm thick gold **ground plane**. The STO film is a lossy dielectric which has a complex permittivity with a dielectric constant and a loss tangent. Both of these parameters are functions of the DC applied electric field (E) and the temperature (T).
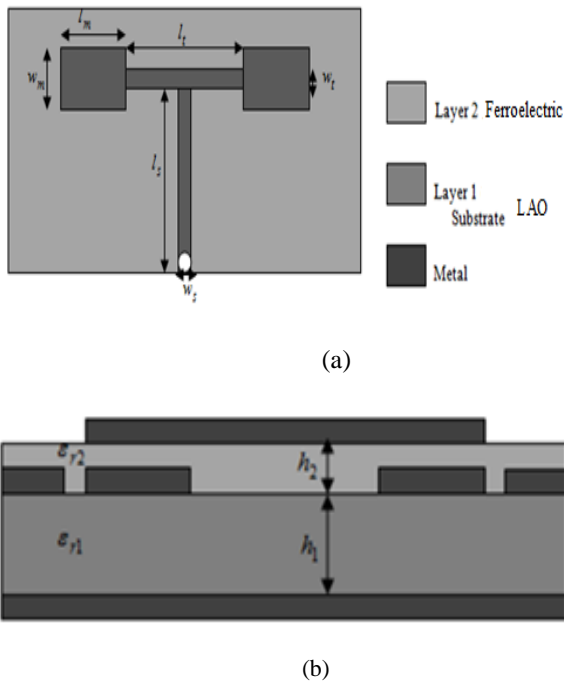

(a)

(b)

*Fig. 11. Layout of ZOR with ferroelectric material
(a) Top view (b) Side view.*

Fig. 12 shows the magnitude of the transmission scattering parameter (S_{21}) for $50\,\Omega$ YBCO/STO/LAO microstrip line CRLH ZOR shown in Fig. 9, with a 0.35 μm STO thin film. It provides the STO permittivity dependence on its thickness. Table 2 summarizes the plotting curves given in Fig. 10(a, b). As we see, for a given frequency, the attenuation increases with film thickness. At higher frequencies, because of the skin depth effect, more RF field is concentrated in the ferroelectric film and less is concentrated in the dielectric substrate, resulting in larger insertion loss. As the value of the ε_r increases, the attenuation also increases. This is a consequence of mismatches resulting from the decrease in Z_o.

Table 2. Parameters Values of Fig.12.

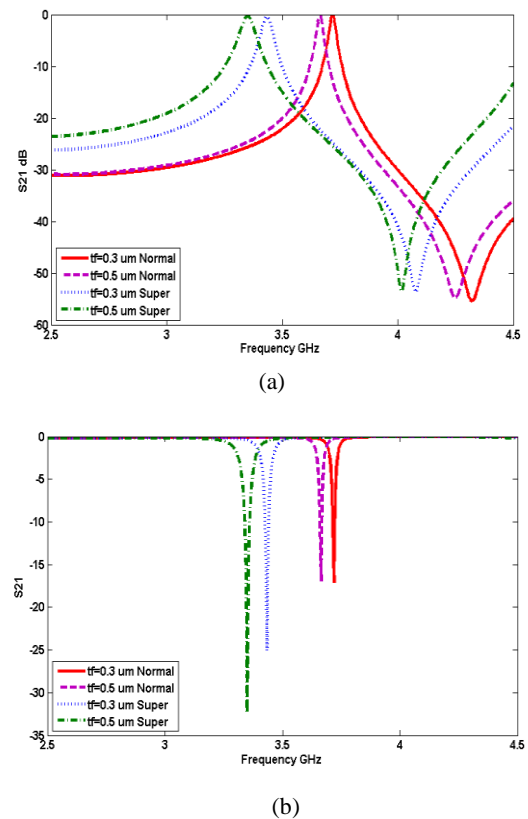| $t_{ferro}(\mu m)$	Normal 300 K		Super 77 K	
	$f_{res}(GHz)$	S21 dB	$f_{res}(GHz)$	S21 dB
0.3	3.715	-0.95	3.435	-0.29
0.5	3.66	-0.97	3.55	-0.34

(a)

(b)

*Fig. 12. Variation of resonance frequency with
ferroelectric thickness t_{ferro}. (a) S_{21} (b) S_{11}.*

Fig. 13 shows the variation of resonance frequency with the temperature which is very attractive at very low temperatures.

Table 3. Parameters Values of Fig. 13.

$T(K)$	ε_r	f (GHz)	S_{21} dB
30	7811	3.41	-0.2
60	2695	3.53	-0.21
77	1867	3.56	-0.22

(a)

(b)
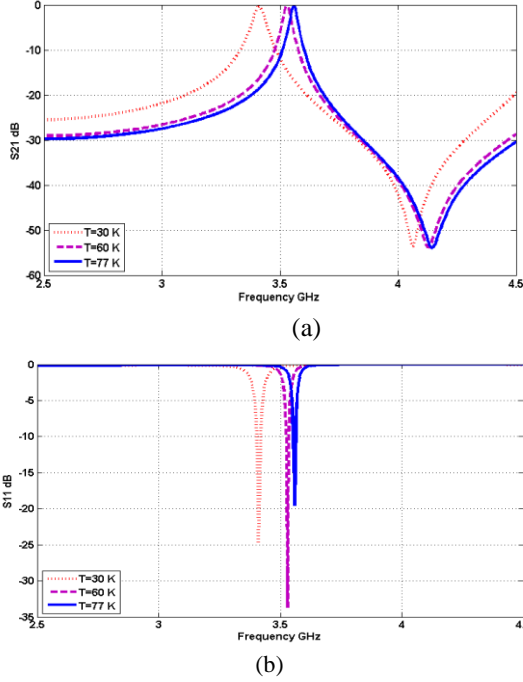
Fig. 13. Variation of resonance frequency with the operating temperature T. (a) S_{21}. (b) S_{11}.

The data were obtained at 77 K in the 2.5 to 4.5 GHz frequency range. Observe that, at no bias and at 3.555 GHz, the insertion loss IL = 0.25 dB. These simulated data are not de-embedded, meaning that any contribution from the SMA launchers used for the measurement to the overall insertion loss has not been subtracted from the data.

Fig. 14 and Table 4 show the effect of E-field on the response of ZOR, the E-fields is changing from 0 to 30 Kv/cm. If one maintains the sample at a constant temperature of 77 K, the ε_r STO is changed from a high value of approximately 1867 at zero bias to a lower value of 741 at a high bias field.

One of the important criteria for the use of ferroelectric thin films in tunable circuits is the large dielectric tunability of the ferroelectric thin film with low additional microwave dielectric losses due to the insertion of the ferroelectric thin films. Dielectric tunability is defined as the (ε_r at zero bias -- ε_r at large bias)/ ε_r at zero bias.

$$n = \frac{\varepsilon_r(E=0) - \varepsilon_r(E)}{\varepsilon_r(E=0)} \qquad (2)$$

Dielectric tunability as high as 90% is attainable in STO thin films at moderate loss-tangent values (typical values between 0.005-0.01 at GHz frequencies). So, this structure will provide a tunability up to 60% for E=30 Kv/cm.

Table 4. Parameters Values of Fig. 14 at T=77 K.

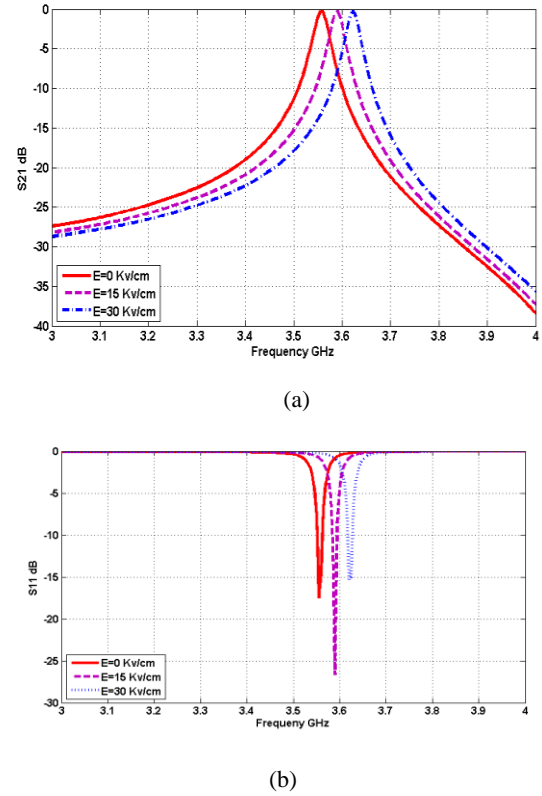| E (Kv/cm)	ε_r	$\tan\delta$ *10^{-4}	f (GHz)	S_{21} dB
0	1867	7.2	3.555	-0.25
15	1168	18.5	3.59	-0.28
30	741	26	3.62	-0.39

(a)

(b)

Fig. 14. Variation of resonance frequency with the applied electric field E. (a) S_{21} (b) S_{11}.

Table 5, demonstrates the comparison between the four proposed structures stated as:-
Case 1: The MIM with a normal conductor (Copper).
Case 2: Adding HTS in replace of Copper to the MIM.
Case 3: Adding the ferroelectric material in case of Copper.
Case 4: Adding the ferroelectric material in case of HTS.

Table 5. A comparative study of the different ZOR structures.

Property		MIM [14]	HTS 77k [Proposed]	Ferro+ Copper [Proposed]	Ferro+ HTS 77k [Proposed]
Perfor.	S_{11}	-10	-34	-18	-32
	S_{21}	-3.55	-0.09	-0.54	-0.023
Tunability		No	No	Yes	Yes
Q factor		1762	43411	9957	68714
Fabrication		Simple	Difficult	Simple	Difficult

5. Conclusions

A compact CRLH ZOR based on MIM structure has been presented. This configuration has been shown to provide high compactness and eliminating the spurious transverse resonances typically existing in the interdigital implementation of the CRLH structure.

Second, an UWB notch filter has been achieved by a CRLH metamaterial unit cell. The desired notch (rejection) band is introduced by a short-circuited resonant circuit connected to the ground. The design parameters were optimized to meet the optimum desired performance.

Last, ZOR CRLH resonator based on ferroelectric was demonstrated in a simulation manner. It is shown that a ferroelectric material may be used for realization of a ZOR providing a different resonance frequency by changing either the applied electric field or the operating temperature.

Acknowledgement

References

[1] V. G. Veselago, Sov. Phys. Uspekhi, **10**, 509 (1968).

[2] A. Shelby, D. R. Smith, S. Schultz, Science, **292**, 77 (2001).

[3] C. Caloz, T. Itoh, Electromagnetic Metamaterials: Transmission Line Theory and Microwave Applications. New York: Wiley-IEEE Press, 2005.

[4] G. V. Eleftheriades, K. G. Balmain, New York: Wiley-IEEE Press, 2005.

[5] N. Engheta, R. W. Ziolkowski, New York, Wiley-IEEE Press, 2006.

[6] R. Marques, F. Martin, M. Sorolla, Hoboken, NJ: Wiley, 2008.

[7] T. J. Cui, R. Liu, D. R. Smith, New York: Springer-Verlag, 2010.

[8] A. Sanada, C. Caloz, T. Itoh, in Proc. Asia–Pacific Microw. Conf., 1588 (2003).

[9] T. Jiang, Y.-J. Feng, J. Zhejiang Univ. Sci., **7**, 76 (2006).

[10] Mahmoud A. Abdalla, Zhirun Hu, IEEE Trans. on Magnetic, **44**(11), (2008).

[11] J.-S. Hong, M. J. Lancaster, John Wiley & Sons, USA, 2001, chapter 7.

[12] R. N. Simons, John Wiley & Sons, USA, 2001, chapter 12.

[13] Yi Wang, Michael J. Lancaster, Frederick Huang, Phe. M. Suherman, Donna M. Holdom, Timothy J. Jackson, IEEE, 2007.

[14] Mohamed M. Mansour, Mostafa A. Elmala, Abdel-Aziz T. Shalaby, El-Sayed M. El-Rabaie, 20th TELFOR 2012, Serbia, Belgerade, 1135 (2012).

_____

[*]Corresponding author: eng_mansor10@yahoo.com